Fotios Kasolis

The Material Distribution Method: Analysis and Acoustics Applications

PhD Thesis

Department of Computing Science
Umeå Univeristy
SE-901 87, Umeå, Sweden

UMINF 14.18
ISSN 0348-0542
ISBN 978-91-7601-122-5
Electronic version available at `http://umu.diva-portal.org`
Typeset by the author with LaTeX
Printed by Print & Media, 2014
Umeå, Sweden 2014

"Whether it’s dusk or dawn’s first light
the jasmine stays always white."

– Giorgos Seferis, *The jasmin*

Dedicated to my mother Stella

Acknowledgements

I would like to thank my scientific advisors Prof. Martin Berggren and Ass. Prof. Eddie Wadbro for their constant encouragement, their patience, and the time they invested in my education. Their effect in the development of my qualifications and skills is considered more than significant and their efforts are deeply appreciated.

Moreover, I would like to thank my parents for their constant support, but more importantly for their motivation is always love; in its most pure form. I am also grateful to Chryssa for being by my side like no other and for revealing to me the significant difference between dreams and obsessions. In addition, I thank my close friends Efi and Roi for many fun and fruitful discussions regarding everything and for their valuable comments on the Greek abstract of this thesis.

Finally, I would like to express my gratitude to my colleagues, here at UMIT Lab, for generously offering the fertile ground for the conditions to thrive and make this work possible.

Fotios Kasolis
Sweden 2014

Abstract

For the purpose of numerically simulating continuum mechanical structures, different types of material may be represented by the extreme values $\{\epsilon, 1\}$, where $0 < \epsilon \ll 1$, of a varying coefficient α in the governing equations. The paramter ϵ is not allowed to vanish in order for the equations to be solvable, which means that the exact conditions are approximated. For example, for linear elasticity problems, presence of material is represented by the value $\alpha = 1$, while $\alpha = \epsilon$ provides an approximation of void, meaning that material-free regions are approximated with a weak material. For acoustics applications, the value $\alpha = 1$ corresponds to air and $\alpha = \epsilon$ to an approximation of sound-hard material using a dense fluid. Here we analyze the convergence properties of such material approximations as $\epsilon \to 0$, and we employ this type of approximations to perform design optimization.

In Paper I, we carry out boundary shape optimization of an acoustic horn. We suggest a shape parameterization based on a local, discrete curvature combined with a fixed mesh that does not conform to the generated shapes. The values of the coefficient α, which enters in the governing equation, are obtained by projecting the generated shapes onto the underlying computational mesh. The optimized horns are smooth and exhibit good transmission properties. Due to the choice of parameterization, the smoothness of the designs is achieved without imposing severe restrictions on the design variables.

In Paper II, we analyze the convergence properties of a linear elasticity problem in which void is approximated by a weak material. We show that the error introduced by the weak material approximation, after a finite element discretization, is bounded by terms that scale as ϵ and $\epsilon^{1/2}h^s$, where h is the mesh size and s depends on the order of the finite element basis functions. In addition, we show that the condition number of the system matrix scales inversely proportional to ϵ, and we also construct a left preconditioner that yields a system matrix with a condition number independent of ϵ.

In Paper III, we observe that the standard sound-hard material approximation with $\alpha = \epsilon$ gives rise to ill-conditioned system matrices at certain wavenumbers due to resonances within the approximated sound-hard material. To cure this defect, we propose a stabilization scheme that makes the condition number of the system matrix

independent of the wavenumber. In addition, we demonstrate that the stabilized formulation performs well in the context of design optimization of an acoustic waveguide transmission device.

In Paper IV, we analyze the convergence properties of a wave propagation problem in which sound-hard material is approximated by a dense fluid. To avoid the occurrence of internal resonances, we generalize the stabilization scheme presented in Paper III. We show that the error between the solution obtained using the stabilized sound-hard material approximation and the solution to the problem with exactly modeled sound-hard material is bounded proportionally to ϵ.

Keywords. Material distribution method, fictitious domain method, finite element method, Helmholtz equation, linear elasticity, shape optimization, topology optimization.

Sammanfattning

I kontinuummekaniska beräkningar kan man representera olika typer av material genom att låta en koefficient α i den aktuella matematiska modellen anta extremvärdena $\{\epsilon, 1\}$, där $0 < \epsilon \ll 1$. För att ekvationerna skall kunna lösas kan inte $\epsilon = 0$ användas, vilket betyder att de exakta fysikaliska villkoren approximeras. För linjär elasticitet betyder $\alpha = 1$ närvaro av material, medan $\alpha = \epsilon$ betyder att frånvaro av material approximeras med ett svagt material. I akustiken motsvarar $\alpha = 1$ närvaro av luft, medan $\alpha = \epsilon$ betyder att ett ljudhårt material approximeras med en högdensitetsfluid. Här analyseras effekterna av denna typ av materialapproximation, och den utnyttjas i syfte att utföra matematisk konstruktionsoptimering.

I artikel I utförs randformsoptimering av ett akustiskt horn. Artikeln introducerar en parameterisering av randen baserad på en lokal, diskret representation av krökningen i kombination med ett fixt beräkningsnät som inte anpassas till den genererade geometrin. Värdet på koefficienten α som används i den matematiska modellen erhålls genom en projektion av den parameteriserade geometrin på det underliggande beräkningsnätet. De optimerade hornen har slät profil och goda transmissionsegenskaper. Den använda parameteriseringen genererar genomgående släta geometrier utan att starka begränsningar på designvariablerna behöver påtvingas.

I artikel II analyseras konvergensegenskaperna för ett linjärt elasticitetsproblem där frånvaro av material approximeras med ett svagt material. Artikeln visar att felet som införs genom materialapproximationen efter finita-elementdiskretisering begränsas av termer som skalar som ϵ och $\epsilon^{1/2}h^s$, där h är nätets elementstorlek och s beror på ordningen av finita-elementfunktionerna. Dessutom visas att systemmatrisens konditionstal är omvänt proportionellt mot ϵ, och en förkonditionerare introduceras som gör systemmatrisens konditionstal oberoende av ϵ.

I artikel III observeras att metoden att approximera ljudhårt material med $\alpha = \epsilon$ ger upphov till illakonditionerade systemmatriser vid vissa vågtal på grund av resonanser i det approximativt ljudhårda materialet. För att åtgärda detta problem föreslås en stabiliseringsmetod som gör konditionstalet oberoende av vågtalet. Dessutom demonstreras att den stabiliserade formuleringen fungerar väl när den används i samband med konstruktionsoptimering av en transmissionskomponent i en akustisk vågledare.

I artikel IV analyseras konvergensegenskaperna för ett vågutbredningsproblem där en ljudhård spridare approximeras med en högdensitetsfluid. För att undvika interna resonanser används en generaliserad version av stabiliteringsmetoden som introducerades i artikel III. Slutsatsen är att felet som introduceras på grund av approximationen skalar proportionellt mot koefficientvärdet ϵ.

Περίληψη

Κατά την αριθμητική προσομοίωση συνεχών μηχανολογικών κατασκευών διαφορετικά υλικά συχνά παριστάνονται από τις ακραίες τιμές $\{\epsilon, 1\}$, όπου $0 < \epsilon \ll 1$, ενός μεταβλητού συντελεστή α που υπεισέρχεται στις εξισώσεις οι οποίες διέπουν το εκάστοτε πρόβλημα. Η παράμετρος ϵ δεν επιτρέπεται να μηδενιστεί, ώστε οι εξισώσεις να είναι επιλύσιμες, γεγονός που οδηγεί στην προσέγγιση ακριβών συνθηκών. Για παράδειγμα, σε προβλήματα γραμμικής ελαστικότητας η παρουσία ύλης αντιπροσωπεύεται από την τιμή $\alpha = 1$, ενώ η τιμή $\alpha = \epsilon$ παράγει μία προσέγγιση του κενού, δηλαδή η απουσία ύλης προσεγγίζεται από ένα ασθενές υλικό. Σε εφαρμογές ακουστικής η τιμή $\alpha = 1$ αντιστοιχεί σε περιοχές κατειλημμένες από αέρα και η τιμή $\alpha = \epsilon$ σε μία προσέγγιση των ηχητικά σκληρών υλικών από κάποιο πυκνό ρευστό. Στην παρούσα διατριβή αναλύουμε τις ιδιότητες σύγκλισης των παραπάνω προσεγγίσεων και χρησιμοποιούμε ανάλογες προσεγγίσεις, ώστε να πραγματοποιήσουμε βελτιστοποίηση γεωμετριών.

Στο Άρθρο Ι διενεργούμε βελτιστοποίηση του σχήματος του συνόρου ενός ακουστικού κέρατος. Προτείνουμε μία παραμετροποίηση που βασίζεται σε μία τοπική, διακριτή καμπυλότητα, την οποία συνδυάζουμε με ένα σταθερό πλέγμα που δεν προσαρμόζεται στα παραγόμενα σχήματα. Οι τιμές του συντελεστή α, ο οποίος υπεισέρχεται στις διέπουσες εξισώσεις, λαμβάνονται με προβολή των παραγόμενων σχημάτων στο υπολογιστικό πλέγμα. Τα βελτιστοποιημένα ακουστικά κέρατα είναι ομαλά και παρουσιάζουν ιδιαίτερα καλές ιδιότητες μετάδοσης. Λόγω της συγκεκριμένης παραμετροποίησης η ομαλότητα των σχημάτων επιτυγχάνεται χωρίς τη χρήση αυστηρών περιορισμών στις μεταβλητές σχεδιασμού.

Στο Άρθρο ΙΙ αναλύουμε τις ιδιότητες σύγκλισης ενός προβλήματος γραμμικής ελαστικότητας, στο οποίο το κενό προσεγγίζεται από ένα ασθενές υλικό. Δείχνουμε ότι, μετά από μία διακριτοποίηση πεπερασμένων στοιχείων, το σφάλμα που υπεισέρχεται από τη χρήση ασθενών υλικών φράσσεται από το άθροισμα όρων ανάλογων του ϵ και του $\epsilon^{1/2}h^s$, όπου h είναι η χαρακτηριστική παράμετρος του πλέγματος και ο αριθμός s εξαρτάται από το βαθμό των συναρτήσεων βάσης των πεπερασμένων στοιχείων. Επιπλέον, δείχνουμε ότι ο καταστατικός αριθμός του προκύπτοντος γραμμικού συστήματος φράσσεται αντιστρόφως ανάλογα του ϵ και κατασκευάζουμε

έναν αριστερό προκλιματιστή που παράγει έναν πίνακα συστήματος καταστατικού αριθμού ανεξάρτητου του ϵ.

Στο Άρθρο III παρατηρούμε ότι η καθιερωμένη προσέγγιση ηχητικά σκληρών υλικών, όπου $\alpha = \epsilon$, οδηγεί σε πίνακες συστήματος δυσμενούς κατάστασης για συγκεκριμένους κυματάριθμους λόγω της εμφάνισης συντονισμών εντός των προσεγγιζόμενων ηχητικά σκληρών υλικών. Για να αποφευχθεί μία τέτοια κατάσταση, προτείνουμε μία μέθοδο σταθεροποίησης που καθιστά τον καταστατικό αριθμό του πίνακα συστήματος ανεξάρτητο του κυματάριθμου. Επιπλέον, δείχνουμε ότι το σταθεροποιημένο πρόβλημα αποδίδει ιδιαίτερα ικανοποιητικά στο πλαίσιο της βελτιστοποίησης της γεωμετρίας μίας ακουστικής συσκευής μετάδοσης.

Στο Άρθρο IV, αναλύουμε τις ιδιότητες σύγκλισης ενός προβλήματος διάδοσης κυμάτων, στο οποίο ένα χωρίο ηχητικά σκληρού υλικού προσεγγίζεται από κάποιο πυκνό ρευστό. Για να αποφευχθεί ο σχηματισμός εσωτερικών συντονισμών, γενικεύουμε τη μέθοδο σταθεροποίησης που παρουσιάσαμε στο Άρθρο III. Δείχνουμε ότι το σφάλμα μεταξύ της λύσης που λαμβάνουμε με χρήση της ευσταθούς προσέγγισης ηχητικά σκληρών υλικών και της λύσης του προβλήματος στο οποίο χρησιμοποιούμε έναν απόλυτα σκληρό σκεδαστή φράσσεται ανάλογα του ϵ.

List of papers*

1. F. Kasolis, E. Wadbro, and M. Berggren.
   Fixed-mesh curvature-parameterized shape optimization of an acoustic horn. *Struct. Multidiscip. Optim.*, 46(5):727–738, 2012.

2. M. Berggren and F. Kasolis.
   Weak material approximation of holes with traction-free boundaries. *SIAM J. Numer. Anal.*, 50(4):1827–1848, 2012.

3. F. Kasolis, E. Wadbro, and M. Berggren.
   Preventing resonances within approximated sound-hard material in acoustic design optimization. *Proceedings of OPT-i 2014*, ISBN: 978-960-99994-5-8, 2014.

4. F. Kasolis, E. Wadbro, and M. Berggren.
   Analysis of fictitious domain approximations of hard scatterers. *Submitted*, 2014.

*The papers have been re-typeset to match the booklets style. There may be minor typographical differences compared to the published papers.

Contents

1 Computational design optimization **19**
1.1 Introduction 19
1.2 Fictitious domain approximations 21
1.3 The material distribution method 23
1.4 Mathematical models 24

2 Summary of papers **29**
2.1 Fixed-mesh curvature parametrized shape opt. of an acoustic horn . 29
2.2 Weak material approximation of holes with traction-free boundaries 32
2.3 Preventing resonances within approximated sound-hard material . . 35
2.4 Analysis of fictitious domain approximations of hard scatterers . . . 38

Paper I
Fixed-mesh curvature parametrized shape optimization of an acoustic horn **47**

Paper II
Weak material approximation of holes with traction-free boundaries **73**

Paper III
Preventing resonances within approximated sound-hard material in acoustic design optimization **101**

Paper IV
Analysis of fictitious domain approximations of hard scatterers **113**

Chapter 1

Computational design optimization

1.1 Introduction

The field of *computational design optimization* combines numerical tools in order to find the values of a set of *design parameters*, connected to the geometrical characteristics of a region subject to design, that result in the best response of a model. The region subject to design is referred to as the *design domain*. As in all mathematical optimization problems, optimal solutions are associated with the extreme values of an *objective function*. Here, we are interested in problems in which the underlying physical state is modeled by partial differential equations. The objective function depends on the geometrical characteristics of the design domain through the solution of a boundary value problem. The goal is to iteratively modify the design domain in order to obtain optimal performance of the model, as measured by the objective function. To abstractly formulate a design optimization problem, we introduce the set $\mathscr{A}$ of feasible designs and we consider a scalar objective function J to be minimized. The design optimization problem then reads:

$$\begin{aligned} &\text{find } \Omega_* \in \mathscr{A} \text{ such that} \\ &J(u(\Omega_*)) \leq J(u(\Omega)) \qquad \forall \Omega \in \mathscr{A}, \end{aligned} \tag{1.1}$$

where constraints on the solution u of the underlying boundary value problem might also be present.

Perhaps the most crucial step during the formulation of a design optimization problem is to choose a mathematical representation of the design domain. Such representations must be suitable for computation. For instance, boundaries can be parameterized using splines [46], or the whole design domain can be parameterized by a domain indicator function [1, 8] or a level set function [42]. Moreover, it is essential to choose a design domain representation that generates a sufficiently large space of candidate designs, relative to the requirements of the application under consideration. In this thesis, we consider *boundary shape* and *topology* optimization problems. In boundary shape optimization problems, the chosen representation of the design grants only variations of a given boundary [45], meaning that topological properties, such as the connectivity, of the final design are the same as those of the initially provided design. In contrast, design representations in topology optimization problems also enable more dramatic modifications, such as changes in the number of holes [8].

Numerical implementations of design optimization problems require approximations of the solution to the underlying boundary value problem for each domain generated by the optimization algorithm. Throughout this thesis, these approximations are obtained using the *finite element method* [13, 14]. For that purpose, we generate a computationally suitable version of the physical domain, such as a truncated variant of an unbounded domain, the so-called *computational domain* and we consider a partition of the computational domain known as *computational mesh*. The solution to the boundary value problem is then approximated by polynomial functions defined on each element of the mesh. Then, design changes that occur during the optimization process have to be incorporated into the software to make the boundary value problem solver aware of the new geometry. These changes can be implemented as deformations of an existing mesh so that the newly generated mesh conforms to each design [36]. Mesh deformations introduce a number of practical complications. First, mesh deformation algorithms are prone to robustness problems. In addition, if we want to provide exact sensitivities of the objective function, we also have to compute sensitivities with respect to mesh deformations [36, 40]. An alternative that does not require domain and mesh changes is provided by so-called *fictitious domain methods* [27].

Design optimization problems can be solved using gradient-based algorithms, such as quasi-Newton methods [41]. To take advantage of the convergence properties of gradient-based algorithms, high accuracy of the computed derivatives is significant. To obtain these derivatives, black-box solutions, such as finite difference methods and algorithmic differentiation [41, Chapter 8], can be used when the number of design variables is small. On the other hand, in medium- and large-scale design optimization problems, these black-box implementations become practically infeasible due to efficiency issues. A situation of particular interest arises when the number of constraints on the solution of the underlying boundary value problem is small. In such cases, the *adjoint method* [22] provides accurate derivatives and has been successfully used in design optimization [32, 33, 44, 51]. More precisely, given a scalar objective function J that depends on a design variable α through the solution u to the linear system $Au(\alpha) = b(\alpha)$, where for the sake of simplicity we assume that the design variable α enters only the right-hand side, the derivative of J with respect to the design variable α is

$$\frac{\partial}{\partial \alpha} J(u(\alpha)) = \left(\frac{\partial J}{\partial u}\right)^{\top} \frac{\partial u}{\partial \alpha} = \left(\frac{\partial J}{\partial u}\right)^{\top} A^{-1} \frac{\partial b}{\partial \alpha}. \tag{1.2}$$

In the adjoint method framework, the vector $(\partial J/\partial u)^{\top} A^{-1}$ is computed by solving the adjoint linear system $A^{\top} v = \partial J/\partial u$. Analogously to the adjoint method, algorithmic differentiation in reverse mode can be used to obtain the exact values for the derivatives of the discrete objective function [41, Chapter 8].

In the 1970s, computational design optimization started being studied as a spin-off of optimal control theory [39], followed by a tendency towards fluid mechanics applications [23, 24, 44]. In 1975, existence of solutions for a domain identification problem was established [17], while a few years later, elasticity applications enter the design optimization arena [18, 34]. One of the first systematic expositions of design optimization for elliptic systems was published in 1984 [45]. In the beginnings, most efforts were directed towards obtaining optimal designs by boundary shape variations. In 1988, one of the most seminal contributions [6], consistent with fictitious domain methods but not presented as such, proposed a method to perform design optimization for elastic structures. There, the authors computed the effective material properties of a material/void composite using a homogenizetion approach and the optimal distribution of this composite. The optimal distribution of the composite was interpreted as the shape of an elastic structure. More recently, other strategies, such as the level set approach [2], have been introduced for topology optimization. Application-wise, design optimization methods have been developed to become an innovative tool in a range of design problems, such as acoustics design [19, 33, 38, 50, 51, 52], antenna design [21, 28, 29], and nanophotonics waveguide design [20].

Computational design optimization is a continuously developing component of the engineering design process and can be used to decrease manufacturing costs and to increase product quality, while at the same time it offers interesting and challenging research problems in each of the involved fields. Recent specialized software, such as Altair OptiStruct, FE-DESIGN Tosca, COMSOL Multphysics, and the Freefem++ toolbox for design optimization, indicate the demand for automated design optimization solutions at an industrial level.

1.2 Fictitious domain approximations

Traditional methods for dealing with multiple, repeated geometrical changes of the computational domain in numerical implementations of boundary value problems can become complicated. Complications arise mainly as part of the necessity to adjust the computational mesh so that it conforms to each generated computational domain. An alternative to the standard approaches of remeshing and mesh deformations is provided by the so-called fictitious domain methods. Fictitious domain methods eliminate the need for mesh adjustments by embedding the original domain into a fixed domain. In addition, the freedom of almost arbitrarily selecting the computational domain enables the use of uniform meshes and thus simplifies implementation.

The main difficulty that arises when using a fictitious domain method is how to impose boundary conditions on the boundary interior to the extended, fictitious domain. In case of essential (Dirichlet) boundary conditions, fictitious domain methods based on Lagrange mutltipliers have been developed [27]. In these methods, mixed variational formulations are constructed, with coupling provided through Lagrange multipliers. This Lagrange multiplier approach shares many features with the finite element Lagrange multiplier formulation for weakly imposing essential boundary conditions [4], which, for strongly elliptic equations, results in saddle-point formulations. Fictitious domain Lagrange multiplier based methods have been studied, among others, for acoustics problems [30, 54]. An alternative to the Lagrange multiplier methods is provided by penalty methods, such as those relying on Nitsche's method for weakly imposing Dirichlet boundary conditions [16, 26, 53].

Throughout our work, we employ a simple fictitious domain approach, commonly used for layout optimization of elastic structures [8], which results in approximations of vanishing natural conditions on the boundaries located in the fictitious domain. More precisely, provided a simply connected domain Ω with a hole ω, as for instance the domain depicted in Figure 1.2, we choose a computational domain $\widehat{\Omega}$ that contains this hole, that is, $\widehat{\Omega} = \Omega \cup \overline{\omega}$. The variational problem is then formulated throughout $\widehat{\Omega}$ and a domain indicator function α with values $\alpha|_{\Omega} = 1$ and $\alpha|_{\omega} = 0$ enters the governing equation. The function α introduces zero-weighted integrals over ω in the variational form, such as

$$\int_{\widehat{\Omega}} \alpha(\,\cdot\,) = \int_{\Omega} 1(\,\cdot\,) + \int_{\omega} 0(\,\cdot\,) = \int_{\Omega} (\,\cdot\,), \tag{1.3}$$

meaning that the equation vanishes in ω and the variational problem essentially reduces to the original problem formulated in Ω. A consequence of zeroing integrals associated with ω is that the α-modified problem is not uniquely solvable since it leaves the solution undetermined within ω. A frequently used cure is to replace the zero value of the indicator function α with a small positive number ϵ. In the context of elasticity and acoustics, such a fictitious domain approach is used to model void and sound-hard scatterers, respectively. As we show in Papers II and IV, this fictitious domain approach provides convergent approximations to the solution of the problems with exactly modeled homogenuous Neumann boundary conditions in the case of a linear elasticity and a wave propagation problem.

1.3 The material distribution method

The material distribution method, which is based on the α-weighted fictitious domain approach discussed in Section 1.2, is commonly used for design optimization. In the material distribution framework, the design variables are mapped to a relaxed version of the material indicator function α that admits values in the interval $[\epsilon, 1]$. This relaxation enables the use of gradient-based algorithms, but, on the other hand, results in designs that are polluted by intermediate values $(\epsilon, 1)$. To obtain almost binary designs, some penalization technique is often used. A popular implicit penalization scheme, the so-called SIMP model, replaces the domain indicator function α with α^s, where the parameter $s > 1$ controls the amount of penalization. In the case of linear elasticity, a volume constraint guarantees that intermediate values are penalized, since they result in structures of low stiffness compared to the amount of used material [7]. An alternative to SIMP is to introduce an explicit penalty term [37], such as a multiple of

$$\int_{\Omega} (\alpha - \epsilon)(1 - \alpha), \tag{1.4}$$

to the objective function.

Usually the penalized problem is ill-posed. As a consequence, numerical solutions will depend on the computational mesh, meaning that it is not possible to obtain a well-defined limiting optimal design by decreasing the mesh size. To recover a well-posed mathematical problem, regularization strategies [10], denoted *design restriction methods*, have been proposed. Design restriction methods exclude from the admissible design set designs of arbitrary fine resolution by bounding, for instance, a perimeter-like measure, or by reducing design fluctuations through filtering. Existence of solutions to a particular design optimization problem under perimeter restriction has been established [3]. When filtering is used as a regularization method, the value of the domain indicator function at each element is replaced by a weighted average over a neighborhood. For the minimal compliance problem of elastic structures, it has been proven that the filtered optimization problem is well-posed [12] and that a well-posedeness property holds also after a finite element discretization [11]. Besides recovering well-posedeness, filtering also prevents the formation of artificial checkerboard patterns [12, 15] when explicitly optimizing over the values of the indicator function α.

1.4 Mathematical models

1.4.1 Acoustic wave propagation

Sound waves are small amplitude longitudinal oscillatory variations in the density of a compressible fluid. Assuming that the perturbation ρ of the fluid density is small compared to the equilibrium density, we can linearize the equations of mass, momentum, and energy conservation. Considering perturbations of an inviscid, quiescent fluid, that is, a uniform fluid at rest, we can relate the density perturbation ρ with the pressure perturbation P through the constitute equation $\rho = P/c^2$, where c is the sound speed. By combining this constitute equation with the linearized equations of motion, we conclude that the acoustic pressure P satisfies the wave equation

$$\frac{\partial^2 P}{\partial t^2} = c^2 \Delta P, \tag{1.5}$$

where Δ is the Laplace operator.

Under the assumption of time harmonic waves with angular frequency ω, it is possible to separate the spatial and temporal components of the acoustic pressure. By combining the separation ansatz $P(x,t) = \operatorname{Re} p(x) e^{\mathrm{i}\omega t}$ with equation (1.5), we conclude that the spatial function p satisfies the equation

$$\Delta p + k^2 p = 0, \tag{1.6}$$

where $k = \omega/c$ is the wavenumber. Solutions of the so-called Helmholtz equation (1.6) are single frequency waves, sometimes called monochromatic waves [35].

For the problems considered in this thesis, equation (1.6) is to be solved on unbounded domains that contain acoustic scatterers and are free from sources at infinity; that is, solutions are assumed to satisfy the Sommerfeld radiation condition [47, 48], which in the two-dimensional case is expressed by

$$\lim_{r\to\infty} \sqrt{r}\left(\mathrm{i}kp + \frac{\partial p}{\partial r}\right) = 0, \tag{1.7}$$

where r is the radial coordinate. Due to finite computational resources, the problems are solved on domains bounded by artificial boundaries. The radiating character of the original problems is approximated through properly chosen strategies, such as perfectly matched layers (PML) or non-reflecting boundary conditions.

In the PML framework the computational domain is equipped with layers of lossy material that are tuned to ensure almost perfect sound attenuation within the fixed width of the layers. A properly manufactured PML makes any sensible terminating boundary conditions, for instance sound-hard conditions, irrelevant regarding its absorbing properties [43]. The presence of such layers of lossy materials in the computational domain leads to the following modified version of equation (1.6),

$$\nabla \cdot (D\nabla p) + k^2\gamma u = 0, \tag{1.8}$$

where, in the two-dimensional case and under the assumption that the PML is terminated by straight boundaries that are aligned with the coordinate system, $D = \mathrm{diag}(\gamma_2/\gamma_1, \gamma_1/\gamma_2)$, $\gamma = \gamma_1\gamma_2$, and γ_1, γ_2 are complex-valued functions different from unity only within the PML region [31].

Another type of a non-reflecting strategy we have extensively used on boundaries terminating infinite waveguides, is the impedance boundary condition

$$\mathrm{i}kp + \frac{\partial p}{\partial n} = g. \tag{1.9}$$

Depending on how the function g is chosen, the corresponding straight boundaries behave as sources and absorbers of planar waves. For instance, if $g = 2\mathrm{i}kA$ for some complex number A, then the corresponding boundary absorbs outgoing planar waves and delivers ingoing planar waves with amplitude A [5]. Note that condition (1.9) constitutes a first order approximation of Sommerfeld's radiation condition (1.7), meaning that its performance as an absorbing condition relies on the number of propagating modes through the waveguide. By choosing the width d of the opening of a waveguide so that $0 < kd < \pi$, we ensure that all non-planar modes are evanescent [9, Subsection 3.5.2] and the artificial boundary at which we impose condition (1.9) is non-reflecting.

Scatterers that consist of sound-hard boundaries, are modeled with the Neumann boundary condition $\partial p/\partial n = 0$. Since acoustic velocity is proportional to the normal derivative of the pressure p, this Neumann boundary condition guarantees that there is no flux through sound-hard boundaries.

For illustration purposes, we construct the following model problem. Let D be the shaded domain depicted in Figure 1.1, in which we consider monochromatic waves governed by equation (1.6). The domain Ω is a scattering object and its boundary $\partial\Omega$ consists of sound-hard walls. On Γ_{in} and Γ_{out} we impose the boundary condition (1.9) with $g = 2\mathrm{i}kA$ and $g = 0$, respectively. If $\partial\mathrm{D}$ denotes the boundary of D, then the sound-hard condition $\partial p/\partial n = 0$ is imposed at $\partial\mathrm{D} \setminus \Gamma$, where $\Gamma = \Gamma_{\mathrm{in}} \cup \Gamma_{\mathrm{out}}$. The variational form of this model problem reads:

$$\begin{aligned}
&\text{find } p \in H^1(\mathrm{D}) \text{ such that}\\
&\int_{\mathrm{D}} \nabla q \cdot \nabla p - k^2 \int_{\mathrm{D}} qp + \mathrm{i}k \int_{\Gamma} qp = 2\mathrm{i}kA \int_{\Gamma_{\mathrm{in}}} q \qquad \forall q \in H^1(\mathrm{D}).
\end{aligned} \tag{1.10}$$

Moreover, it can be shown that the solution to problem (1.10) satisfies the equa-

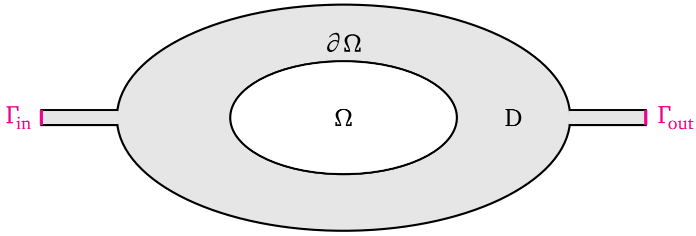

Figure 1.1: The domain setup for the model Helmholtz problem (1.10).

tion

$$\int_{\Gamma_{\mathrm{in}}} |A|^2 - \int_{\Gamma_{\mathrm{in}}} |p-A|^2 = \int_{\Gamma_{\mathrm{out}}} |p|^2. \tag{1.11}$$

Equation (1.11) can be interpreted as an energy balance equation stating that the portion of the energy that enters the domain D through Γ_{in} is reflected back to Γ_{in} and the rest of it is leaving the domain through the boundary Γ_{out}. Hence, it is relevant to define the wavenumber dependent *reflection coefficient* R_k on Γ_{in} as the quotient between the amplitude $\langle p\rangle_{\Gamma_{\mathrm{in}}} - A$, where $\langle p\rangle_{\Gamma_{\mathrm{in}}}$ is the average value of p at Γ_{in}, of the reflected wave and the amplitude A of the incoming wave, that is,

$$R_k = \frac{\langle p\rangle_{\Gamma_{\mathrm{in}}} - A}{A}. \tag{1.12}$$

Given wavenumber k, the transmission properties of the device can be characterized by the amplitude and phase of the complex number R_k. The model presented here is relevant to Papers I, III, and IV.

1.4.2 Linear elastostatics

Linear elasticity is the theory of small deformations of elastic structures under loads [25]. We consider the elastic body depicted in Figure 1.2. The body occupies a domain Ω and contains a hole ω. The boundary of Ω is denoted $\partial\Omega$. The equilibrium deformation is determined by a balance of the effective force density, here assumed to vanish inside Ω. Hence, the governing equation

$$-\nabla\cdot(E\nabla u) = 0 \qquad \text{in } \Omega, \tag{1.13}$$

where $E\nabla u = \sigma$ is the linearized stress tensor, u is the displacement field, and E is the fourth-order elasticity tensor. For homogenous and isotropic bodies the following constitute equation holds;

$$E\nabla u = \lambda I(\nabla\cdot u) + \mu\left[\nabla u + (\nabla u)^\top\right], \tag{1.14}$$

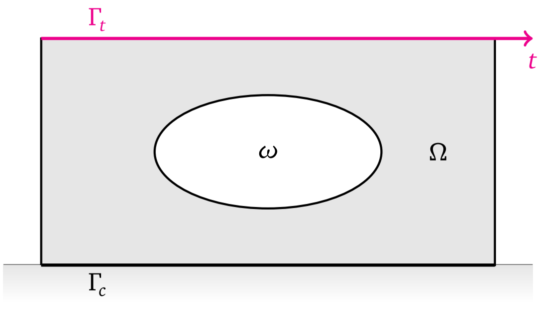

Figure 1.2: The domain setup for the linear elasticity problem (1.15).

where μ and λ are the so-called Lamé parameters. If the body is fixed along Γ_c, then $u|_{\Gamma_c} = 0$. To impose a surface traction load t along Γ_t and the traction-free boundaries $\partial\Omega \setminus \{\Gamma_c \cup \Gamma_t\}$, as shown in Figure 1.2, we set the boundary conditions $n \cdot (E\nabla u) = t$ and $n \cdot (E\nabla u) = 0$, respectively. The variational form of the linear elasticity problem under consideration reads:

$$
\begin{aligned}
&\text{find } u \in V \text{ such that} \\
&\int_\Omega \nabla v \cdot E\nabla u = \int_{\Gamma_t} v \cdot t \qquad \forall v \in V,
\end{aligned}
\tag{1.15}
$$

where $V = \left\{ v \in H^1(\Omega) \mid v|_{\Gamma_c} = 0 \right\}$. In the context of the α-weighted fictitious domain method presented in Section 1.2, this linear elasticity model is used for the analysis in Paper II.

Chapter 2

Summary of papers

2.1 Paper I: Fixed-mesh curvature parametrized shape optimization of an acoustic horn

2.1.1 Problem statement

We optimize the shape of a planar acoustic horn in free space with respect to reflections measured at a waveguide attached to the horn's throat. The computational setup is depicted in Figure 2.1. The governing boundary value problem consists of Helmholtz equation (1.8) with impedance conditions (1.9), where $g = 2\mathrm{i}kA$ at the truncated waveguide boundary Γ_{in}, and sound-hard conditions elsewhere. The computational domain $\widehat{\Omega}$ contains the PML region as well as the domains Ω and Ω_{d} that are occupied by air and sound-hard material, respectively. Following the α-weighted fictitious domain approach presented in Section 1.2, a coefficient α_h is used for representing the horn domain Ω_{d}, The variational form of the problem under consideration reads:

$$\begin{aligned}&\text{find } p_h \in V_h \text{ such that}\\ &\int_{\widehat{\Omega}} \alpha_h \nabla q \cdot (D_h \nabla p_h) - k^2 \int_{\widehat{\Omega}} \alpha_h \gamma_h q p_h \\ &\qquad + \mathrm{i}k \int_{\Gamma_{\mathrm{in}}} q p_h = 2\mathrm{i}kA \int_{\Gamma_{\mathrm{in}}} q \qquad \forall q \in V_h,\end{aligned} \tag{2.1}$$

where V_h is the space of continuous, element-wise biquadratic functions. We specify the design boundary Γ_{d} by introducing a curvature-based parametrization as describe below. Given Γ_{d}, we generate a domain Ω_{d}, represented and incorporated in the governing equation through the coefficient α_h. The optimization problem regards minimization of reflections back to the feeding boundary Γ_{in} for a set of wavenumbers K and reads:

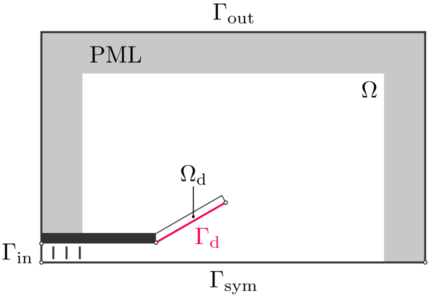

Figure 2.1: The computational domain for the horn problem.

$$\min_{\vartheta \in \Theta} \frac{1}{2} \sum_{k \in K} |R_k|^2 + \frac{\mu}{2} \|\vartheta\|^2 \text{ subject to (2.1)} \tag{2.2}$$

where ϑ is a vector containing the design variables, Θ is the set of admissible designs, and R_k is the reflection coefficient defined by equation (1.12). The term $\mu\|\vartheta\|^2/2$, where $\mu > 0$, introduces a Tikhonov regularization.

2.1.2 Main contributions and outcomes

We propose a flexible curvature-based parameterization combined with a fictitious domain approach. Let Γ_{d} be the boundary subject to design. We define Γ_{d} as a set of S connected line segments, of fixed length ℓ, that form a polygonal line. The design variables are chosen to be the angle differences ϑ_j between adjacent line segments. Note that ϑ_j/ℓ constitutes a discrete measure of the local curvature of Γ_{d}. Given Γ_{d}, we generate a design domain Ω_{d} using the offset vectors $w(n_j+n_{j+1})/2$, where w is the width of the sound-hard material used to form the waveguide and n_j are the normals to the line segments comprising Γ_{d}, as illustrated in Figure 2.2 (left). The back side $\partial\Omega_{\mathrm{d}} \setminus \Gamma_{\mathrm{d}}$ of the horn is not individually parameterized, since computational experience suggests that its shape is of minor importance with respect to the considered performance measure. Given Ω_{d}, we define the values of α_h by

$$\alpha_h|_{E_n} = 1 + (\epsilon - 1)\frac{|E_n \cap \Omega_{\mathrm{d}}|}{|E_n|}, \tag{2.3}$$

where $|\cdot|$ denotes the area of the corresponding set, E_n is the n-th element of the computational mesh, and $0 < \epsilon \ll 1$ is a parameter characterizing the domain Ω_{d}. According to expression (2.3), elements which are entirely contained in Ω_{d} are assigned the value ϵ, while elements for which $E_n \cap \Omega_{\mathrm{d}} = \emptyset$ are assigned the value one. For the rest of the elements, that is, elements that contain a portion of the design boundary Γ_{d}, equation (2.3) interpolates between the values ϵ and one according to the relative fraction of each element E_n that lies in Ω_{d}.

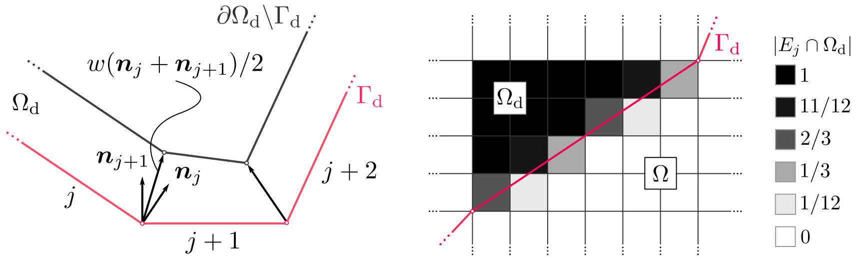

Figure 2.2: (Left) The back side of the horn is generated by linear interpolation of the offset vectors $w(n_j + n_{j+1})/2$. (Right) The values of the area $|E_n \cap \Omega_d|$ used to find the values of the function a_h.

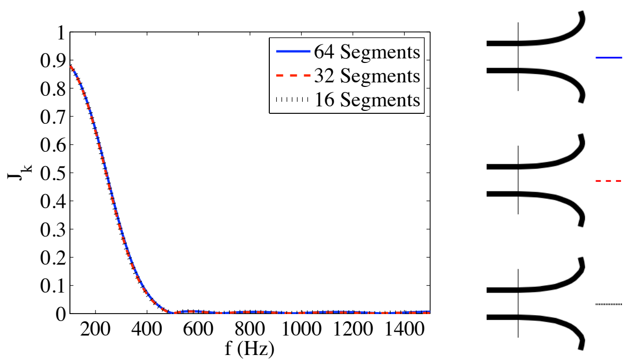

Figure 2.3: Optimal horns for 466–1480 Hz and their corresponding spectra. The horn pixel-based representations correspond (from top to bottom) to 64, 32, and 16 design variables and the horn length is $|\Gamma_d| = 0.4$ m in all cases.

Figure 2.2 (right) depicts an illustrative example of the mapping (2.3) for a single line segment.

In this contribution, we solve the nonlinear least squares optimization problem (2.2) using Matlab's routine `lsqnonlin`, which implements an interior, trust-region algorithm with Gauss–Newton Hessian approximations. We fix the sound-hard parameter ϵ at 10^{-8}, and we perform experiments using 64, 32, and 16 design variables. Figures 2.3 and 2.4 depict horns optimized over the bands of frequencies 466–1480 Hz and 293–392 Hz, respectively. The resulting horns transmit remarkably well for the bands they were optimized, as can be seen from their reflection spectra in the same figures. Moreover, our experiments indicate that there exists a limiting design with increasing number of design variables.

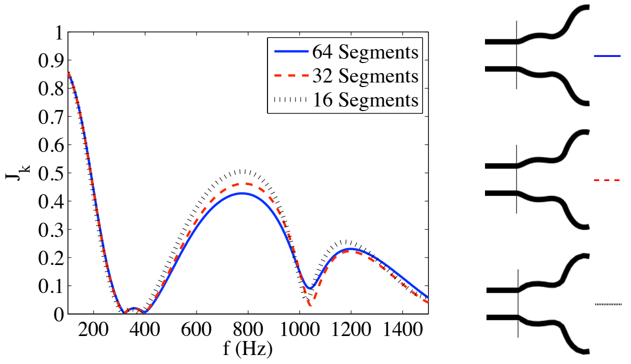

Figure 2.4: Optimal horns for 293–392 Hz and their corresponding spectra. The horn pixel-based representations correspond (from top to bottom) to 64, 32, and 16 design variables and the horn length is $|\Gamma_\mathrm{d}| = 0.4$ m in all cases.

2.2 Paper II: Weak material approximation of holes with traction-free boundaries

2.2.1 Problem statement

We consider the linear elasticity problem discussed in Subsection 1.4.2 under the fictitious domain framework presented in Section 1.2. For that purpose, we introduce a material indicator function ρ, with values $\rho|_\Omega = 1$ and $\rho|_\omega = \epsilon$ in the material and material-free regions Ω and ω, respectively. The discrete weak material approximation problem then reads:

$$\begin{aligned}
&\text{find } u_h^\epsilon \in \widehat{V}_h \text{ such that} \\
&\int_{\widehat{\Omega}} \rho \nabla v \cdot (E \nabla u_h^\epsilon) = \int_{\Gamma_t} v \cdot t \qquad v \in \widehat{V}_h,
\end{aligned} \tag{2.4}$$

where $\widehat{\Omega} = \Omega \cup \overline{\omega}$ and $\widehat{V}_h$ is the space of continuous, element-wise polynomial functions. Recall that the weak material parameter $0 < \epsilon \ll 1$ is chosen to circumvent the problem of having a vanishing equation in ω, which would leave the solution undetermined in ω. Here, we study the solution error introduced by the weak-material approximation and the conditioning of the corresponding system when a finite element discretization is used.

2.2.2 Main contributions and outcomes

We prove that there is a constant $C > 0$ such that the error $\|u - u_h^\epsilon\|_{1,\Omega}$ between the solution u of problem (1.15) and the solution u_h^ϵ of the weak material approximation problem (2.4) satisfies

$$
\begin{aligned}
C\|u-u_h^\epsilon\|_{1,\Omega} \le &\inf_{v\in V_h}\|u-v\|_{1,\Omega} \\
&+\epsilon^{1/2}\inf_{v\in V_h}\|u^\omega-v\|_{1,\omega}+\epsilon\|\lambda(u^\omega)\|_{-1/2,\partial\Omega},
\end{aligned}
\tag{2.5}
$$

where u^ω is the continuous elastic extension of u in ω and $\lambda(u^\omega)$ is the surface traction on the boundary $\partial\omega$ of ω from the inside. Using a finite element discretization of problem (2.4), we show that, in case of quasi-uniform meshes, there exists a constant $C>0$ such that the condition number $\kappa(A_\epsilon)$ of the resulting system matrix A_ϵ is bounded as

$$
\kappa(A_\epsilon)\le Ch^{-2}\epsilon^{-1} \tag{2.6}
$$

for all $\epsilon\in(0,1/2]$, where $h\in(0,1]$ is the mesh parameter. In addition, provided a node numbering that corresponds to nodes in Ω, $\partial\Omega$, and ω sequentially, we introduce the scaling matrix

$$
D_\epsilon=\operatorname{diag}[I_{N_\Omega},(1+\epsilon)I_{N_{\partial\omega}},\epsilon I_{N_\omega}], \tag{2.7}
$$

where N_Ω, $N_{\partial\omega}$, and N_ω denote the number of the nodal values within the subscripted sets. Moreover we show that the condition number $\kappa(\widetilde{A}_\epsilon)$, where $\widetilde{A}_\epsilon = D_\epsilon^{-1}A_\epsilon$, is bounded independent of the weak material parameter ϵ as

$$
\kappa(\widetilde{A}_\epsilon)\le Ch^{-2} \tag{2.8}
$$

and that the limit matrix $\widetilde{A}_0=\lim_{\epsilon\to0}\widetilde{A}_\epsilon$ is well defined.

We solve problem (1.15) using a fine triangulation ($h\approx 0.015$) of the domain Ω depicted in Figure 2.5 (left) and we denote the solution as u_{ref}. The weak material approximation problem (2.4) is then solved with and without using the preconditioner (2.7) over the extended domain $\widehat{\Omega}$, which also contains the void regions ω, shown in Figure 2.5 (right) together with one of the used meshes.

In Figure 2.6 we present the error in the semi-norm $|u_{\text{ref}}-u_h^\epsilon|_{1,\Omega}$ which, for large ϵ values, is dominated by the weak material approximation term. Note that the slope of the error curve tends to $O(\epsilon)$ as we decrease the discretization error by using finer meshes. For $\epsilon\le 10^{-4}$, the error is dominated by the finite element bound $O(h)$.

Figure 2.7 shows the dependence of the condition numbers $\kappa(A_\epsilon)$ and $\kappa(\widetilde{A}_\epsilon)$ on the weak material parameter ϵ. We observe that the condition number $\kappa(A_\epsilon)$ exhibits a growth inversely proportional to ϵ, whereas $\kappa(\widetilde{A}_\epsilon)$ is almost constant throughout the studied range of ϵ, and, furthermore, it is well conditioned as $\epsilon\to0$.

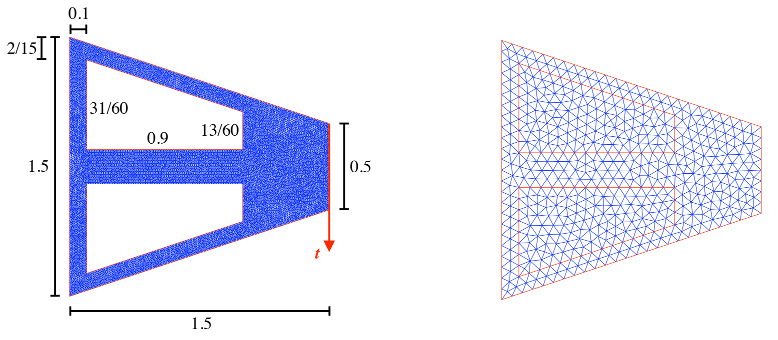

Figure 2.5: (Left) The domain in which the original problem (1.15) is considered and a finite element approximation u_{ref} is obtained. (Right) One of the triangulations ($h \approx 0.082$) used to solve problem (2.4) over the extended domain $\widehat{\Omega}$ which also contains the void regions.

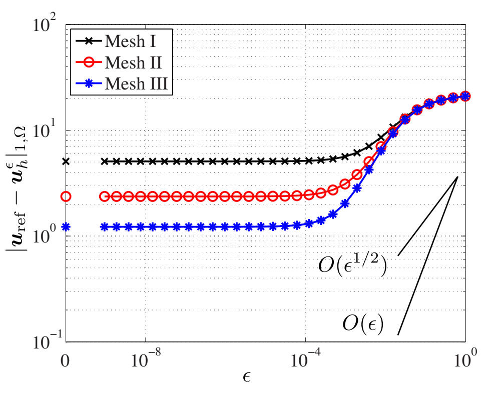

Figure 2.6: The error $|u_{\text{ref}} - u_h^{\epsilon}|_{1,\Omega}$ as a function of ϵ for three meshes with $h \approx 0.082$ (Mesh I), $h \approx 0.045$ (Mesh II), and $h \approx 0.026$. The isolated points to the left indicate the error for the limit problem with system matrix $\widetilde{A}_0$.

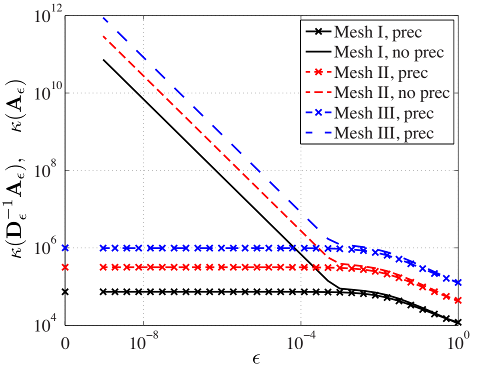

Figure 2.7: The condition number of the non-preconditioned (lines) and the preconditioned (crosses) matrices as a function of the weak material parameter ϵ. The asterisks indicate the condition number for the limit problem with system matrix $\widetilde{A}_0$.

2.3 Paper III: Preventing resonances within approximated sound-hard material in acoustic design optimization

2.3.1 Problem statement

We study the effect of the material distribution approach to topology optimization for the Helmholtz equation of acoustics. The variational form of the problem under consideration is (1.10) for the domain depicted in Figure 2.8 (right), where D, Ω, Γ_{in}, and Γ_{out} have been replaced with Ω, Ω_{H}, Γ_{L} and Γ_{R}, respectively. Employing the α-weighted fictitious domain method presented in Section 1.2, we introduce a function α_h such that $\alpha_h = 1$ whenever air is present and $0 < \alpha_h = \epsilon \ll 1$ in regions filled with sound-hard material. Hence the solution of problem (1.10) is approximated with the solution of the sound-hard material approximation problem:

$$
\begin{aligned}
&\text{find } p_h \in V_h \subset H^1(\Omega) \text{ such that}\\
&\int_{\hat{\Omega}} \alpha_h \nabla q \cdot \nabla p_h - k^2 \int_{\hat{\Omega}} \alpha_h q p_h \\
&\qquad + ik \int_{\Gamma_{\text{L}}\cup\Gamma_{\text{R}}} q p_h = 2ikA \int_{\Gamma_{\text{L}}} q \qquad \forall q \in V_h,
\end{aligned}
\tag{2.9}
$$

where $\hat{\Omega} = \Omega \cup \overline{\Omega}_{\text{H}}$, V_h consists of continuous, element-wise polynomial functions on a meshing of $\hat{\Omega}$, and α_h is an element-wise constant function with values $\alpha_h \in [\epsilon, 1]$, $0 < \epsilon \ll 1$. The extreme values ϵ and one correspond to regions filled with sound-hard material and air, respectively. The objective is to find the

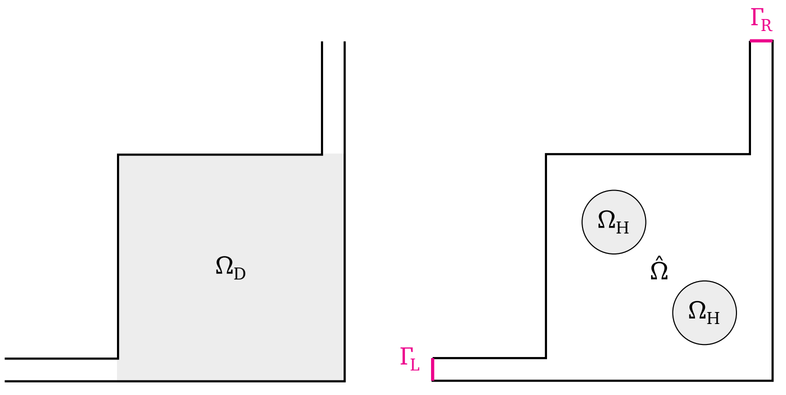

Figure 2.8: (Left) Physical waveguide bend. (Right) Truncated waveguide bend.

distribution of sound-hard material in the design domain Ω_D shown in Figure 2.8 that minimizes reflections back to Γ_L for a set of wavenumbers. For that purpose we solve the problem

$$\min_{\tilde{\alpha}_h} \left[\frac{1}{2} \sum_k R_k^2(\alpha_h) + J_\gamma(\alpha_h) \right] \text{ subject to (2.9),} \tag{2.10}$$

where the reflection coefficients R_k are given by equation (1.12). The penalty term

$$J_\gamma(\alpha_h) = \gamma \int_\Omega (\alpha_h^s - \epsilon)(1 - \alpha_h^s) \tag{2.11}$$

promotes designs that solely consist of sound-hard material and air depending on the penalty parameter $\gamma \geq 0$ and it implicitly controls the amount of sound-hard material in the final designs through the biasing parameter $s \in (0, 1]$. The design variable $\tilde{\alpha}_h$ is defined through the filter

$$\alpha_h(x) = \int_{\mathbb{R}^2} \tilde{\alpha}_h(y) \Phi_\tau(x, y) \mathrm{d}y, \tag{2.12}$$

where the filter kernel Φ_τ is cone-shaped within radius τ, for the reasons discussed in Section 1.3.

2.3.2 Main contributions and outcomes

Formulation (2.9) can become ill-conditioned due to the occurrence of resonances in regions of sound-hard material. Resonances, associated with the eigenmodes of the Laplacian, can appear in the sound-hard region for certain frequencies. To cure this issue, we weight the mass integral within sound-hard material so that the conditioning of the finite element system improves. The proposed change

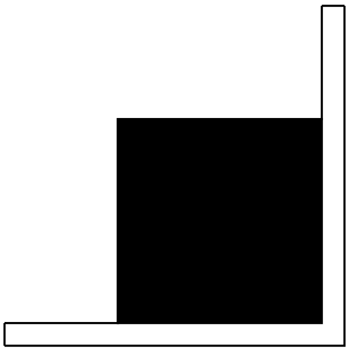

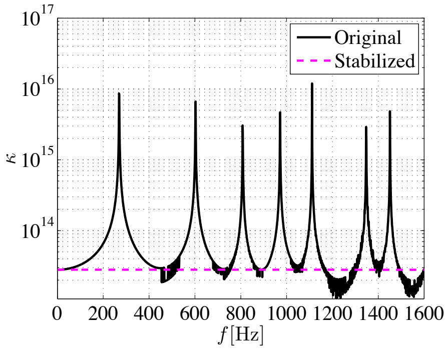

Figure 2.9: (Left) The design used to test occurence of resonances, where white corresponds to air and black corresponds to approximated sound-hard material. (Right) The condition number of the system matrices for the original and the stabilized problem for the design to the left of the figure.

enforces an effective increment of the wavelength for small values of α_h, so that the formation of resonances becomes irrealizable within the sound-hard material. Our modification replaces the coefficient α_h in the mass integral of (2.9) with the coefficient α_h^2, resulting in the stabilized variational form:

$$\int_{\Omega} \alpha_h \nabla q \cdot \nabla p_h - k^2 \int_{\Omega} \alpha_h^2 q p_h + ik \int_{\Gamma_\mathrm{L} \cup \Gamma_\mathrm{R}} q p_h = 2ikA \int_{\Gamma_\mathrm{L}} q. \tag{2.13}$$

The sound-hard approximation problems (2.9) and (2.13) are solved using nine-node square elements with $h = 3.125$ mm and $\epsilon = 10^{-8}$. For the domain depicted in Figure 2.9 (left), we observe that the condition number, depicted to the right in the same figure, of the system matrix that corresponds to (2.9) exhibits peak values for certain frequencies. In contrast, when the proposed formulation (2.13) is used, the condition number effectively becomes independent of the wavenumber k.

The optimal designs shown in Figure 2.10, are obtained with the method of moving asymptotes [49] combined with a continuation approach, as explained in the paper, with respect to the coefficient γ in the penalty term (2.11), where we set $s = 1/4$ to avoid an observed tendency of the optimization algorithm to place material close to the openings of the waveguides. The corresponding reflection spectra in dB, $R = 20\log_{10}|R_k|$ with R_k given by (1.12), are depicted in Figure 2.11 and indicate that, when using the stabilized problem, the optimization algorithm was able to find a local minimum with better performance than when the unstabilized problem was used. The stabilization also improves the performance of the optimization algorithm in terms of number of iterations.

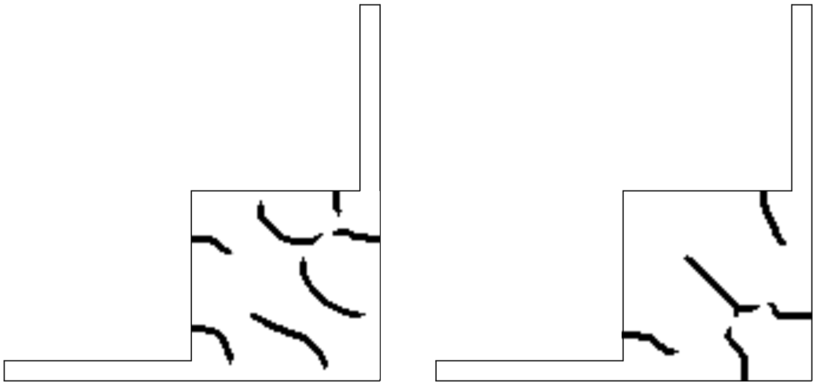

Figure 2.10: Optimal designs for frequencies $f(n) = 220 \cdot 2^{n/12}$ for $n = 3, 4, \ldots, 14$ when using (left) the original problem and (right) the stabilized one.

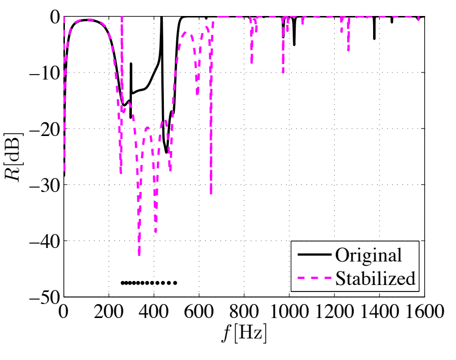

Figure 2.11: Reflection spectra of the optimal designs depicted in figure 2.10. The dots indicate the frequencies for which we optimize.

2.4 Paper IV: Analysis of fictitious domain approximations of hard scatterers

Here we analyze an α-weighted fictitious domain wave propagation problem, analogous to the one presented for the linear elasticity problem studied in Paper II. However, since the bilinear form of the problem studied here is not strongly coercive, the analysis becomes more involved. In addition, the difficulty observed in Paper III, that is, the occurrence of resonances within the approximated sound-hard scatterer, further complicates the study. For these reasons, we choose to limit our analysis to the convergence properties of the fictitious domain approximation of a scatterer in the continuous case, before discretization.

2.4.1 Problem statement

We consider the domain setup depicted in Figure 2.12. The domain for the Helmholtz equation is D and the problem is supplied with the boundary conditions discussed in Section 1.4.1. The associated variational problem reads:

$$\begin{aligned}&\text{find } p^{\mathrm{D}} \in H^1(\mathrm{D}) \text{ such that}\\ &a^{\mathrm{D}}(q,p^{\mathrm{D}}) = \ell(q) \quad \forall q \in H^1(\mathrm{D}),\end{aligned} \tag{2.14}$$

where

$$\begin{aligned} a^{\mathrm{D}}(q,p^{\mathrm{D}}) &= \int_{\mathrm{D}} \nabla q \cdot \nabla p^{\mathrm{D}} - k^2 \int_{\mathrm{D}} q p^{\mathrm{D}} + \mathrm{i}k \int_{\Gamma} q p^{\mathrm{D}},\\ \ell(q) &= \int_{\Gamma_{\mathrm{in}}} q g,\end{aligned} \tag{2.15}$$

and $\Gamma = \Gamma_{\mathrm{in}} \cup \Gamma_{\mathrm{out}}$.

In the context of the α-weighted fictitious domain method presented in Section 1.2, we use a coefficient α to represent the scattering object that occupies Ω. The values of α are $\alpha|_{\Omega} = \epsilon$, where $0 < \epsilon \ll 1$, and $\alpha|_{\mathrm{D}} = 1$. This fictitious domain approximation of the hard scatterer in Ω results in the following problem.

$$\begin{aligned}&\text{Find } p_\epsilon \in H^1(\widehat{\mathrm{D}}) \text{ such that}\\ &a_\epsilon(q,p_\epsilon) = \ell(q) \quad \forall q \in H^1(\widehat{\mathrm{D}}),\end{aligned} \tag{2.16}$$

where $\widehat{\mathrm{D}} = \mathrm{D} \cup \overline{\Omega}$, $a_\epsilon(q,p_\epsilon) = a^{\mathrm{D}}(q,p_\epsilon) + \epsilon a_\epsilon^{\Omega}(q,p_\epsilon)$, and

$$a_\epsilon^{\Omega}(q,p_\epsilon) = \int_{\Omega} \nabla q \cdot \nabla p_\epsilon - \eta(\epsilon) k^2 \int_{\Omega} q p_\epsilon. \tag{2.17}$$

For $\eta(\epsilon) = \epsilon$ we recover the stabilization scheme introduced in Paper III in order to prevent the occurrence of resonances interior to the approximated hard-scatterer.

2.4.2 Main contributions and outcomes

We generalize the stabilization technique introduced in Paper III by providing conditions on the function η so that it acts as stabilization against resonances within the scatterer. Moreover, we show that the stabilized fictitious domain formulation provides convergent approximations of the solution p^{D} to problem (2.14) and we study the error introduced in view of the fictitious domain approximation.

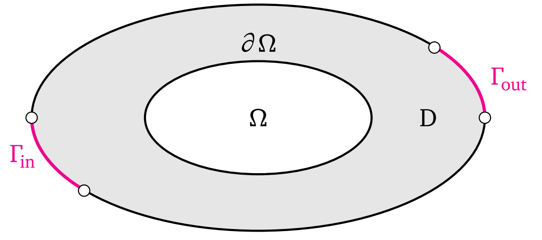

Figure 2.12: Conceptual domain setup for the Helmholtz problem (2.14).

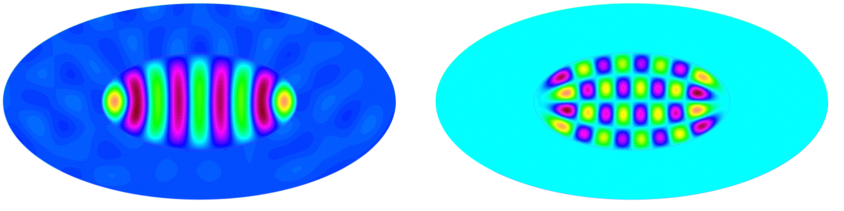

Figure 2.13: The occurrence of resonances within the scattering object, when solving problem (2.16) with $\eta(\epsilon) = 1$, that is following the standard framework presented in Section 1.2.

We prove that if $\eta(\epsilon) < 2/(k^2 \text{diam}^2 \Omega)$, then there exists a constant $c > 0$ such that

$$\sup_{q \in H^1(\widehat{\mathrm{D}}) \setminus \{0\}} \frac{\operatorname{Re} a_\epsilon(q, p)}{\|q\|_{1,\epsilon}} \geq c \|p\|_{1,\epsilon} \tag{2.18}$$

for each $\epsilon \in (0, 1/2]$, where the ϵ-norm is defined by $\|\cdot\|^2_{1,\epsilon} = \|\cdot\|^2_{1,\mathrm{D}} + \epsilon \|\cdot\|^2_{1,\Omega}$. The inf-sup condition (2.18) implies that the solution p_ϵ of problem (2.16) restricted in D approaches the solution p^{D} of problem (2.14) as $\epsilon \to 0$. In addition, the restriction of p_ϵ in the scatterer Ω, that is $p_\epsilon|_\Omega$, approximates the solution of the following continuous Helmholtz extension problem:

$$\begin{aligned} &\text{find } p^\Omega_\epsilon \in H^1(\Omega) \text{ such that } \gamma^\Omega p^\Omega_\epsilon = \widetilde{\gamma}^{\mathrm{D}}_{\partial\Omega} p^{\mathrm{D}}|_{\partial\Omega} \text{ and} \\ &a^\Omega_\epsilon(q, p^\Omega_\epsilon) = 0 \quad \forall q \in H^1(\Omega), \end{aligned} \tag{2.19}$$

where γ^Ω and $\widetilde{\gamma}^{\mathrm{D}}_{\partial\Omega}$ are the trace operators from Ω and D on the boundary $\partial\Omega$ of the scatterer, respectively. The proof of the inf-sup condition (2.18) relies on uniqueness of solutions to problem (2.19), imposed by choosing functions η that satisfy $\eta(\epsilon) < 2/(k^2 \text{diam}^2 \Omega)$. In addition, by using condition (2.18), we show that the stabilized problem (2.16) provides linearly convergent approximations of the solution p^{D} to problem (2.14), in which the scatterer is exactly modeled, that is,

$$\|p^{\mathrm{D}} - p_\epsilon\|_{1,\epsilon} \leq \epsilon C \|p^{\mathrm{D}}\|_{1,\mathrm{D}}. \tag{2.20}$$

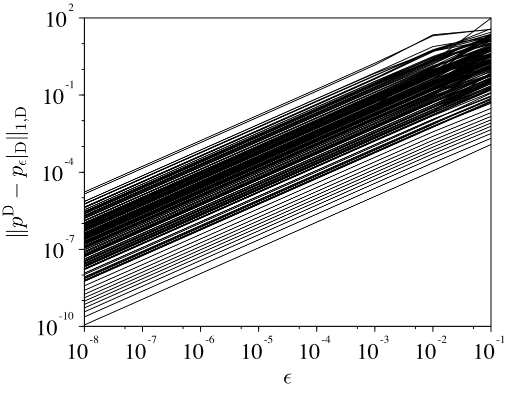

Figure 2.14: The error $\|p^{\mathrm{D}}-p_{\epsilon}|_{\mathrm{D}}\|_{1,\mathrm{D}}$ as a function of the sound-hard material parameter ϵ for wavenumbers $k = 20\pi n/c$, $n = 1, 2, \ldots, 15, 16$.

In Figure 2.14, we plot the error $\|p^{\mathrm{D}} - p_{\epsilon}|_{\mathrm{D}}\|_{1,\mathrm{D}}$ as a function of the parameter ϵ using logarithmic scale for both axes. Each line corresponds to a wavenumber $k = 20\pi n/c$, where $c = 343$ and $n = 1, 2, \ldots, 15, 16$. The slope of the depicted lines tends to one as $\epsilon \to 0$, numerically confirming estimate (2.20).

Bibliography

[1] G. Allaire. *Shape optimization by the homogenization method.* Springer, 2002.

[2] G. Allaire, F. Jouve, and A.-M. Toader. Structural optimization using sensitivity analysis and a level-set method. *J. Comput. Phys.*, 194(1):363–393, 2004.

[3] L. Ambrosio and G. Buttazzo. An optimal design problem with perimeter penalization. *Calc. Var. Partial Differential Equations*, 1(1):55–69, 1993.

[4] I. Babuška. The finite element method with Lagrangian multipliers. *Numer. Math.*, 20(3):179–192, 1973.

[5] E. Bängtsson, D. Noreland, and M. Berggren. Shape optimization of an acoustic horn. *Comput. Methods Appl. Mech. Engrg.*, 192(11–12):1533–1571, 2003.

[6] M. P. Bendsøe and N. Kikuchi. Generating optimal topologies in structural design using a homogenization method. *Comput. Methods Appl. Mech. Engrg.*, 71(2):197–224, 1988.

[7] M. P. Bendsøe and O. Sigmund. Material interpolation schemes in topology optimization. *Arch. Appl. Mech.*, 69(9–10):635–654, 1999.

[8] M. P. Bendsøe and O. Sigmund. *Topology optimization: theory, methods and applications.* Springer, 2003.

[9] J. Billingham and C. King. *Wave motion.* Cambridge University Press, 2006.

[10] T. Borrvall. Topology optimization of elastic continua using restriction. *Arch. Comput. Method. E.*, 8(4):351–385, 2001.

[11] T. Borrvall and J. Petersson. Topology optimization using regularized intermediate density control. *Comput. Methods Appl. Mech. Engrg.*, 190(37–38):4911–4928, 2001.

[12] B. Bourdin. Filters in topology optimization. *Int. J. Numer. Meth. Engng.*, 50(9):2143–2158, 2001.

[13] D. Braess. *Finite elements: theory, fast solvers, and applications in solid mechanics*. Cambridge University Press, 2001.

[14] S. C. Brenner and R. Scott. *The mathematical theory of finite element methods*. Springer, 2008.

[15] T. E. Bruns and D. A. Tortorelli. Topology optimization of non-linear elastic structures and compliant mechanisms. *Comput. Methods Appl. Mech. Engrg.*, 190(26–27):3443–3459, 2001.

[16] E. Burman and P. Hansbo. Fictitious domain finite element methods using cut elements: II. a stabilized Nitsche method. *Appl. Numer. Math.*, 62(4):328–341, 2012.

[17] D. Chenais. On the existence of a solution in a domain identification problem. *J. Math. Anal. Appl.*, 52(2):189–219, 1975.

[18] K.-T. Cheng and N. Olhoff. An investigation concerning optimal design of solid elastic plates. *Int. J. Solids Struct.*, 17(3):305–323, 1981.

[19] M. B. Dühring, J. S. Jensen, and O. Sigmund. Acoustic design by topology optimization. *J. Sound Vib.*, 317(3–5):557–575, 2008.

[20] Y. Elesin, F. Wang, J. Andkjær, J. S. Jensen, and O. Sigmund. Topology optimization of nano-photonic systems. In *Advanced Photonics Congress*, page IM2B.4. Optical Society of America, 2012.

[21] A. Erentok and O. Sigmund. Topology optimization of sub-wavelength antennas. *IEEE Trans. Antennas Propagat.*, 59(1):58–69, 2011.

[22] M. B. Giles and N. A. Pierce. An introduction to the adjoint approach to design. *Flow Turbul. Combust.*, 65(3–4):393–415, 2000.

[23] R. Glowinski and O. Pironneau. On the numerical computation of the minimum-drag profile in laminar flow. *J. Fluid Mech.*, 72(2):385–389, 1974.

[24] R. Glowinski and O. Pironneau. Toward the computation of minimum drag profiles in viscous laminar flow. *Appl. Math. Model.*, 1:58–66, 1976.

[25] M. E. Gurtin. *An introduction to continuum mechanics*. Elsevier Science, 1982.

[26] P. Hansbo. Nitsche's method for interface problems in computational mechanics. *GAMM-Mitteilungen*, 28(2):183–206, 2005.

[27] J. Haslinger and R. A. E. Mäkinen. *Introduction to shape optimization: theory, approximation, and computation*. SIAM, 2003.

[28] E. Hassan, E. Wadbro, and M. Berggren. Conductive material distribution optimization for ultrawideband antennas. In *Proceedings 11th International Conference on Mathematical and Numerical Aspects of Waves : Waves 2013*, pages 171–172. ENIT-LAMSIN, 2013.

[29] E. Hassan, E. Wadbro, and M. Berggren. Topology optimization of uwb monopole antennas. In *7th European Conference on Antennas and Propagation (EuCAP2013)*, Proceedings of the European Conference on Antennas and Propagation, pages 1488–1492, 2013.

[30] E. Heikkola, Y. A. Kuznetsov, P. Neittaanmäki, and J. Toivanen. Fictitious domain methods for the numerical solution of two-dimensional scattering problems. *J. Comput. Phys.*, 145(1):89–109, 1998.

[31] E. Heikkola, T. Rossi, and J. Toivanen. Fast direct solution of the Helmholtz equation with a perfectly matched layer or an absorbing boundary condition. *Int. J. Numer. Meth. Engng.*, 57(14):2007–2025, 2003.

[32] A. Jameson, L. Martinelli, and N. A. Pierce. Optimum aerodynamic design using the Navier–Stokes equations. *Theor. Comp. Fluid Dyn.*, 10(1–4):213–237, 1998.

[33] F. Kasolis, E. Wadbro, and M. Berggren. Fixed-mesh curvature-parameterized shape optimization of an acoustic horn. *Struct. Multidiscip. O.*, 46(5):727–738, 2012.

[34] N. Kikuchi, K. Y. Chung, T. Torigaki, and J. E. Taylor. Adaptive finite element methods for shape optimization of linearly elastic structures. *Comput. Methods Appl. Mech. Engrg.*, 57(1):67–89, 1986.

[35] L. D. Landau and E. M. Lifshitz. *Fluid mechanics*. Elsevier Science, 1959.

[36] E. Laporte and P. Tallec. *Numerical methods in sensitivity analysis and shape optimization*. Birkhäuser Boston, 2003.

[37] G. K. Lau, H. Du, and M. K. Lim. Techniques to suppress intermediate density in topology optimization of compliant mechanisms. *Comput. Mech.*, 27(5):426–435, 2001.

[38] J. W. Lee and Y. Y. Kim. Topology optimization of muffler internal partitions for improving acoustical attenuation performance. *Int. J. Numer. Meth. Eng.*, 80(4):455–477, 2009.

[39] J. L. Lions. *Optimal control of systems governed by partial differential equations*. Springer-Verlag, 1971.

[40] B. Mohammadi and O. Pironneau. *Applied shape optimization for fluids*. Oxford University Press, 2010.

[41] J. Nocedal and S. J. Wright. *Numerical optimization*. Springer, 2006.

[42] S. Osher and A. J. Sethian. Fronts propagating with curvature dependent speed: algorithms based on Hamilton–Jacobi formulations. *J. Comput. Phys.*, 79(1):12–49, 1988.

[43] P. G. Petropoulos. On the termination of the perfectly matched layer with local absorbing boundary conditions. *J. Comput. Phys.*, 143(2):665–673, 1998.

[44] O. Pironneau. On optimum design in fluid mechanics. *J. Fluid Mech.*, 64(1):97–110, 1974.

[45] O. Pironneau. *Optimal shape design for elliptic systems*. Springer-Verlag, 1984.

[46] J. A. Samareh. Survey of shape parameterization techniques for high-fidelity multidisciplinary shape optimization. *AIAA Journal*, 39(5):877–884, 2001.

[47] S. H. Schot. Eighty years of Sommerfeld's radiation condition. *Historia Math.*, 19(4):385–401, 1992.

[48] A. Sommerfeld. Die Greensche funktion der Schwingungsgleichung. *Jhrber. Deutsch. Math.-Verein*, 21:309–353, 1912.

[49] K. Svanberg. The method of moving asymptotes — a new method for structural optimization. *Int. J. Numer. Meth. Eng.*, 24(2):359–373, 1987.

[50] R. Udawalpola, E. Wadbro, and M. Berggren. Optimization of a variable mouth acoustic horn. *Int. J. Numer. Meth. Eng*, 85(5):591–606, 2011.

[51] E. Wadbro and M. Berggren. Topology optimization of an acoustic horn. *Comput. Method. Appl. M.*, 196(1–3):420–436, 2006.

[52] E. Wadbro, R. Udawalpola, and M. Berggren. Shape and topology optimization of an acoustic horn-lens combination. *J. Comput. Appl. Math.*, 234(6):1781–1787, 2010.

[53] E. Wadbro, S. Zahedi, G. Kreiss, and M. Berggren. A uniformly well-conditioned, unfitted Nitsche method for interface problems. *BIT*, 53(3):791–820, 2013.

[54] Y. Zhang. A fictitious domain method for acoustic wave propagation problems. *Math. Comput. Modelling*, 50(3–4):351–359, 2009.